PROCEEDINGS, Thirty-Fourth Workshop on Geothermal Reservoir Engineering
Stanford University, Stanford, California, February 9-11, 2009
SGP-TR-187

THREE-DIMENSIONAL POROELASTIC SIMULATION OF HYDRAULIC AND NATURAL FRACTURES USING THE DISPLACEMENT DISCONTINUITY METHOD

X. X. Zhou and A. Ghassemi

Texas A&M University
3116 TAMU-401E Richardson Building
College Station, TX, USA
e-mail: ahmad.ghassemi@pe.tamu.edu

ABSTRACT

A three-dimensional fully-coupled poroelastic displacement discontinuity method is developed and used to analyze the temporal variation of opening and slip of a natural fracture in a reservoir in response to the sudden application of fluid pressure in the fracture surfaces. Numerical results show that a hydraulic fracture opens in an increasing manner with time as the rock moves towards a drained state under the applied stress. The applied pore pressure induces a time-dependent closure caused by the rock dilation. On the other hand, poroelastic analysis of a natural fracture subjected to shear shows that the fracture slip decreases with the time in response to a pore pressure-induced increase in the normal stresses on the joint.

THEORY OF POROELASTICITY

One of the main features of the deformation of fluid-saturated porous rock is its transient nature which is related to the presence of a fluid diffusion process, and is described by the linear theory of poroelasticity (Biot, 1941). Since the pioneering work of Biot, the theory of poroelasticity has been reformulated by a number of investigators, such as Rice and Cleary (1976), and Carroll (1980).

The coupled constitutive equations of poroelastic material under isothermal conditions are (e.g., Rice & Cleary, 1976):

$$\varepsilon_{ij} = \frac{1}{2G}\left[\sigma_{ij} - \frac{v}{1+v}\sigma_{kk}\delta_{ij}\right] + \frac{\alpha(1-2v)}{2G(1+v)}\delta_{ij}p \quad (1)$$

$$\zeta = \frac{\alpha(1-2v)}{2G(1+v)}\sigma_{kk} + \frac{\alpha^2(1-2v)^2(1+v_u)}{2G(1+v)(v_u-v)}p \quad (2)$$

where ε_{ij} and σ_{ij} are respectively the strain and stress of the solid matrix, p and ζ are respectively the pore pressure and pore volume, δ_{ij} is the Kronecker delta. The material constants are the shear modulus G, Biot coefficient α, the drained and undrained Poisson's ratios v and v_u, Skempton's pore pressure coefficient B. These equations describe the fundamental aspects of the deformation of fluid-saturated porous rock namely; (i) the sensitivity of the volumetric response of the rock to pore pressure changes and thus the rate of loading, and (ii) variation of pore pressure due to the application of a mean stress.

The three-dimensional filed equations for the poroelastic rock deformation can be presented as a Navier equation with a coupling term, and a diffusion equation:

$$G\nabla_2^2 u_i + \frac{G}{1-2v}u_{k,ki} - \alpha p_{,i} = 0 \quad (3)$$

$$\frac{\partial p}{\partial t} - \frac{2\kappa GB^2(1-2v)(1+v_u)^2}{9(v_u-v)(1-2v_u)}\nabla_3^2 p = -\frac{2GB(1+v_u)}{3(1-2v_u)}\frac{\partial \varepsilon}{\partial t} \quad (4)$$

where u_i is the solid displacement in the i direction, ε is the volumetric strain, and the other notations are the same as those defined previously.

DISPLACEMENT DISCONTINUITY METHOD

The displacement discontinuity (DD) method is an indirect boundary element method which is based on the fundamental solutions of a point DD in an infinite elastic or poroelastic medium. This technique has been used extensively in mining and hydraulic fracturing (Crouch and Starfield, 1983; Vandamme, 1989; Ghassemi and Roegiers, 1996). It is a boundary

method and has the advantage of reducing the dimensions of the problem by one. The formulation of DD can be based on the solution of a constant line or square DD in an infinite elastic medium (Crouch and Starfield, 1981). Alternatively, a point displacement DD can be integrated over an area (square, triangle or quadrilateral) to form elements which form the building block of the DD method. The stresses and displacements due to a three dimensional point DD in a poroelastic medium is given by Carvalho and Curran (1998) and Cheng and Detournay (1998).

A fracture in a poroelastic medium can be viewed as a surface across which the solid displacements and the normal fluid flux are discontinuous. The DDs and fluid sources are then distributed along the fracture surface such that the superposition of their effects satisfies the prescribed boundary conditions at the fracture surface. Given the DDs and fluid sources, the stresses and pore pressure at any point in the reservoir rock may be evaluated using the principle of superposition:

$$\sigma_{ij}(\mathbf{x},t)=\int_0^t\int_A\begin{Bmatrix}\sigma_{ijkn}^{id}(\mathbf{x}-\mathbf{x}',t-t')D_{kn}(\mathbf{x}',t')+\\ \sigma_{ij}^{is}(\mathbf{x}-\mathbf{x}',t-t')D_f(\mathbf{x}',t')\end{Bmatrix}dA(\mathbf{x}')dt'+\sigma_{ij0}(\mathbf{x}) \tag{5}$$

$$p(\mathbf{x},t)=\int_0^t\int_A\begin{Bmatrix}p_{ij}^{id}(\mathbf{x}-\mathbf{x}',t-t')D_{ij}(\mathbf{x}',t')+\\ p^{is}(\mathbf{x}-\mathbf{x}',t-t')D_f(\mathbf{x}',t')\end{Bmatrix}dA(\mathbf{x}')dt'+p_0(\mathbf{x}) \tag{6}$$

where D_{kn} (or D_{ij}) and D_f are the displacement discontinuity and the fluid source intensity, respectively; σ_{ijkn}^{id}, σ_{ij}^{is}, p_{ij}^{id} and p^{is} are the instantaneous fundamental solutions, *i.e.*, the stresses and pore pressures due to a unit impulse of the displacement discontinuity ("*id*") in the *kn*-direction and a unit impulse of the fluid source intensity ("*is*"); and σ_{ij0} and p_0 are the initial stresses and pore pressure. Eqs. (5) and (6) are applied on the fracture surface to obtain the solution system. For planar fractures, the normal stresses at the fracture depend only on the normal component of DD; while the shear stresses on the fracture depend only upon the shear components of DD. Also, the fluid source intensity on the fracture contributes only to the normal stresses but not the shear stress on the *fracture surface*, and only the normal components of DD contribute to the pore pressures at the *fracture surface (z=0)*. Therefore, the traction components at the fracture surface can be written as:

$$\sigma_{zz}(\mathbf{x},t)=\int_0^t\int_A\begin{Bmatrix}\sigma_{zzzz}^{id}(\mathbf{x}-\mathbf{x}',t-t')D_{zz}(\mathbf{x}',t')+\\ \sigma_{zz}^{is}(\mathbf{x}-\mathbf{x}',t-t')D_f(\mathbf{x}',t')\end{Bmatrix}dA(\mathbf{x}')dt'+\sigma_{zz0}(\mathbf{x}) \tag{7}$$

$$p(\mathbf{x},t)=\int_0^t\int_A\begin{Bmatrix}p_{zz}^{id}(\mathbf{x}-\mathbf{x}',t-t')D_{zz}(\mathbf{x}',t')+\\ p^{is}(\mathbf{x}-\mathbf{x}',t-t')D_f(\mathbf{x}',t')\end{Bmatrix}dA(\mathbf{x}')dt'+p_0(\mathbf{x}) \tag{8}$$

in the normal direction, and

$$\sigma_{zx}(\mathbf{x},t)=\int_0^t\int_A\begin{Bmatrix}\sigma_{zxzx}^{id}(\mathbf{x}-\mathbf{x}',t-t')D_{zx}(\mathbf{x}',t')+\\ \sigma_{zxzy}^{id}(\mathbf{x}-\mathbf{x}',t-t')D_{zy}(\mathbf{x}',t')\end{Bmatrix}dA(\mathbf{x}')dt'+\sigma_{zx0}(\mathbf{x}) \tag{9}$$

$$\sigma_{zy}(\mathbf{x},t)=\int_0^t\int_A\begin{Bmatrix}\sigma_{zyzx}^{id}(\mathbf{x}-\mathbf{x}',t-t')D_{zx}(\mathbf{x}',t')+\\ \sigma_{zyzy}^{id}(\mathbf{x}-\mathbf{x}',t-t')D_{zy}(\mathbf{x}',t')\end{Bmatrix}dA(\mathbf{x}')dt'+\sigma_{zy0}(\mathbf{x}) \tag{10}$$

in the shear directions, where *z*-axis is in the normal direction of the fracture surface, *x*-axis and *y*-axis are perpendicular and in the fracture surface plane.

Eqs. (7)-(8) can be solved together to obtain the DDs in the normal direction and fluid source intensities; thereafter, Eqs. (9)-(10) are solved to obtain the DDs in the shear directions. Once the DDs and fluid source intensities on the fracture surface are determined, Eqs. (7)-(10) can then be used to calculate the stresses and pore pressure at any location in the rock matrix.

In general, the integral equation presented above cannot be solved analytically and therefore, a numerical procedure is required. In this work, the fracture is discretized into a number of four-noded quadrilateral elements in the spatial domain, which makes the integrals over the whole fracture be replaced by a sum of integrals over these elements. The DDs are assumed to be constant over each element which facilitates the treatment of the hypersingular integrations involved; while the fluid source intensities are assumed to vary linearly over each element. In the time domain, the DDs and source intensities are assumed to be constant over each time step, and the space integral are performed numerically.

The above procedure can be used to study both hydraulic fractures and joints. A hydraulic fracture usually is pressurized in excess of the minimum in-situ stress and remains open during the loading process, which means both the normal and shear stiffness of the fracture are zero. On the hydraulic fracture surface, the normal tractions equal the fluid pressures in the fracture and the shear tractions equal zero. However, a different approach must be used for joints, as the joint normal and shear stiffness are nonzero and the normal and shear tractions on a joint change with joint normal and shear displacements.

The procedure for modeling the joint element is similar to that used by Ghassemi et al. 2007, however, the fracture is discretized into a number of four-nodded quadrilateral elements in this work. During the fracture pressurization, each element can be either in a state of "separation", "stick" or "slip"; the element is closed in the latter two states.

In this paper, we denote the normal stiffness of the fracture as K_n. The shear stiffness of the fracture may be different in different shear directions. However, here we assume the shear stiffnesses are the same in all shear directions for simplification and denote it as K_s. The fracture aperture increment for any closed element "i" can be expressed as:

$$\Delta \overset{i}{d}_n = \overset{i}{D}_{zz} + \overset{i}{a}_{dil} = \left(\frac{-\Delta \overset{i}{\sigma}'_n}{\overset{i}{K}_n} \right) + \overset{i}{a}_{dil} \qquad (11)$$

where $\Delta \overset{i}{\sigma}'_n$ is the increment of the normal effective stress and $\overset{i}{a}_{dil}$ is the dilation-induced aperture increase due to shear slip. In this work, for simplification, we assume the shear dilation is the same in all shear slip directions. As a result, the shear dilation for any element "i" may be simply calculated by the following relation:

$$\overset{i}{a}_{dil} = \sqrt{\overset{i}{D}_{zx}^2 + \overset{i}{D}_{zy}^2} \tan\left(\overset{i}{\phi}_{dil} \right) \qquad (12)$$

where $\overset{i}{D}_{zx}$ and $\overset{i}{D}_{zy}$ are the shear displacement components in x and y direction, respectively and $\overset{i}{\phi}_{dil}$ is the fracture dilation angle.

MODEL VERIFICATION

To verify the numerical model, we compare its predictions with the available analytical solutions for the penny-shaped crack problem. Sneddon (1946) solved the problem of an infinitely thin crack subjected to uniform normal traction p applied to its faces. The fracture opening in the normal direction is given by:

$$w(r) = \frac{4(1-v)\,pa}{\pi G} \sqrt{1-(r/a)^2} \qquad (13)$$

where a is the radius of the fracture, r is the radius of the computational point, G is the shear modulus, and v is the Poisson's ratio. Also, Segedin (1950) solved the problem of an infinitely thin penny-shaped fracture whose faces are subjected to uniform shearing tractions, S. The ride of the fracture in the direction of the shear force is given by:

$$u(r) = \frac{8(1-v)Sa}{\pi G(2-v)} \sqrt{1-(r/a)^2} \qquad (14)$$

where all the notations are the same as those in Eq. (13).

The material is assumed to be linear elastic in both Eq. (13) and (14). However, in our numerical model, the material is poroelastic meaning that the fracture aperture would be time dependent. To compare the two solutions, we consider the drained poroelastic response from the numerical solution, corresponding to a very large time when the pore pressures in the rock almost completely dissipate (here we use 10^8s for a rock with 10^{-15}m^2 of permeability). We set the shear modulus and Poisson's ratio of the material to 4000 MPa and 0.25, respectively. Fig. 1 shows the fracture mesh which contains 800 four-noded quadrilateral elements and 841 nodes. The size of typical elements is around 1.5×1.5 m^2 and the time increment is 10^6s in the computation.

Fig. 2 shows the comparisons between the numerical and analytical solutions for the opening of the fracture under a unit uniform normal traction. The results for the fracture ride under a unit uniform shear tractions applied at the fracture surface are shown in Figure 3. Generally the numerical results agree well with the analytical results. The error of the numerical results increases near the fracture tip; this is caused by the use of constant elements instead of special tip elements.

NUMERICAL SIMULATIONS

We consider a horizontal circular planar fracture in a poroelastic rock. The fracture is subject to a suddenly applied, constant fluid pressure $p = 15$ MPa at time $t = 0$. It is assumed that the initial stresses in the filed are isotropic and the vertical and horizontal components are 30 MPa and 20 MPa, respectively. The fracture normal stiffness modulus of the fracture is assumed to be 10^8 Pa/m. The problem can be decomposed into two sub-problems corresponding to two types of the loading (Carter and Booker, 1982): Mode 1, a normal stress loading $\sigma_n = pH(t)$; and Mode 2, a pore pressure loading $p = pH(t)$, where $H(t)$ denotes the Heaviside step function. The mesh used for this part contains 1047 four-noded quadrilateral element and 1100 element nodes.

Fig. 4 shows the evolution of the fracture aperture in the middle of the central fracture element in response to Mode 1 loading. Note that the fracture opens with time as the pore pressure that is initially generated in the porous rock gradually dissipates. The fracture response under Mode 2 is illustrated in Fig. 5; the fracture closes progressively starting from zero to a stabilized value after a long time. This phenomenon

is caused by the rock dilation when the fluid leaks-off from the fracture into the reservoir matrix.

Fig. 6 shows the fracture aperture profiles for the complete problem (both Modes 1 and 2) for the undrained and drained cases. In the undrained case, we let t=100s in the numerical simulation so that there is almost no pore pressure dissipation or fluid leak-off from the fracture into the rock; while in the drained case, we let $t=10^8$s in order to allow both of Modes 1 and 2 transient processes to be complete. Note that the fracture aperture in the early time (undrained) case is larger than that of the large time (drained) response because of the effect of Mode 2 which induces a fracture closure.

In the following, we analyze the opening and slip of a planar fracture that is subjected to a fluid pressure which is less than the in-situ minimum stress. This condition can be expected when stimulating geothermal reservoirs. The fracture surface has a dip angle of 60° and its strike direction is parallel to the local x-axis. It is assumed that the fracture is in an in situ stress of σ_v=60.13MPa, σ_{hmin}=34.81MPa, σ_{Hmax}=50.88MPa, and p=17.4MPa (Ghassemi et al., 2007). The orientation of σ_{Hmax} is parallel to the fracture strike direction. This stress field can be rotated to the local fracture coordinate system to obtain σ_{zz}=41.1MPa, σ_{xz}=0MPa, and σ_{yz}=11.0MPa. It is also assumed that the effective friction angle and dilation angle of the fracture are 30° and 3°, respectively. Both the normal and shear stiffness of the fracture are assumed to be 10^{10} Pa/m. The other material properties used here are shown in Table 1.

In the numerical model, the fracture is discretized into a mesh with 1834 four-noded quadrilateral elements and 1919 element nodes as shown in Fig. 7. For simplicity, we assume the fluid pressure in the fracture is constant and uniform and its value is 25MPa. Figs 8-11 show the simulation results for the variations of fracture aperture, shear slip in the x-direction, shear slip in the y-direction, and the normal effective stress on element B (see Fig. 7). Figure 8 illustrates the fracture aperture variation on element B with time; indicating a fracture closure. As can be seen in Figures 9 and 10, the magnitudes of the shear slip in both the x-direction and y-direction decrease with the passage of the time. This is an interesting result made possible by our analysis; it can be explained by the increase of the normal stresses with time. The joint closure and shear strength are directly proportional to the normal effective stress at the fracture surface. The normal effective stress increases (Figure 11) in response the matrix dilation due to fluid leak-off from the fracture into the reservoir matrix and constraint dilation.

Table 1. Data set used in the numerical example.

Parameter	**Value**
Shear modulus G (GPa)	4.0
Poisson's ratio v	0.25
Fluid viscosity μ_f (N.s/m^2)	0.001
Fluid diffusivity c_f (m^2/s)	10^{-3}
Biot's coefficient α	0.95
Fluid density ρ_f (kg/m^3)	1000
Rock density ρ_r (kg/m^3)	2650
Rock permeability κ (m^2)	10^{-16}

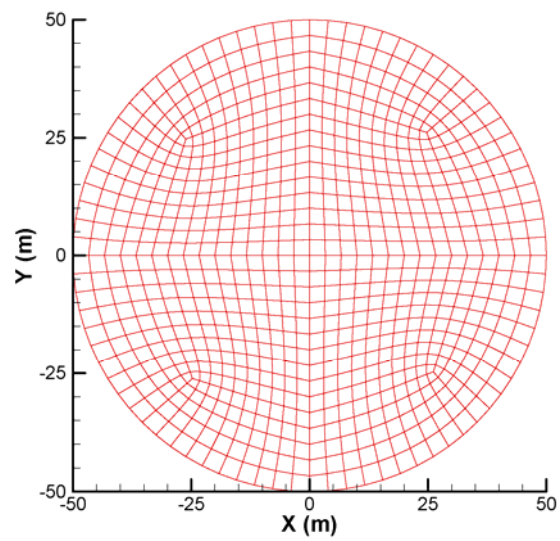

Figure 1: Mesh for the circular fracture example used to verify the numerical model.

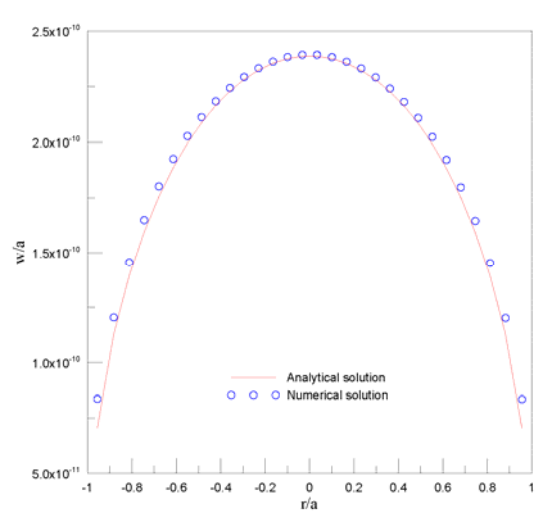

Figure 2: Comparisons between numerical and analytical results for fracture opening.

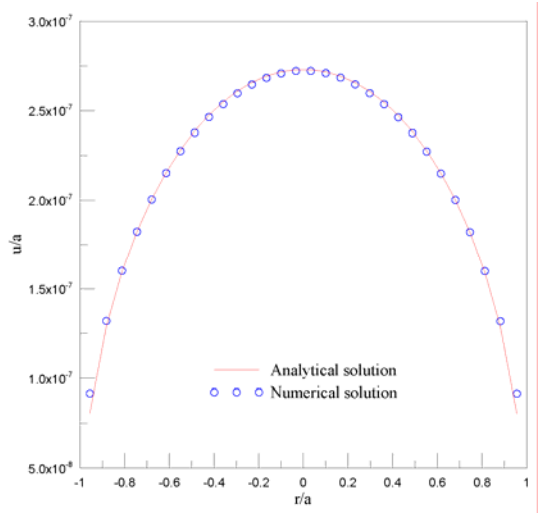

Figure 3: Comparisons between numerical and analytical results for fracture slip in shear.

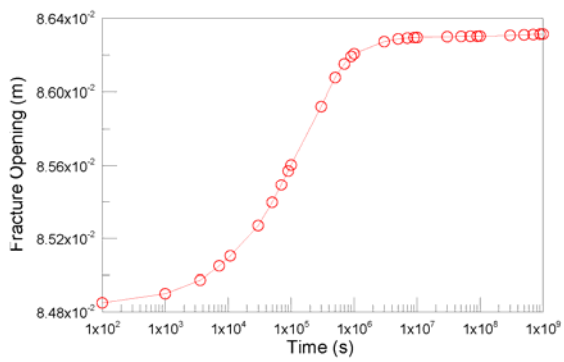

Figure 4: Variations of fracture opening with time at element A due to Model.

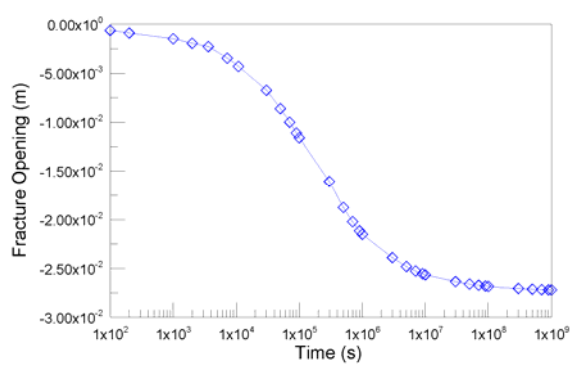

Figure 5: Variations of fracture opening with time at element A due to Mode 2 loading.

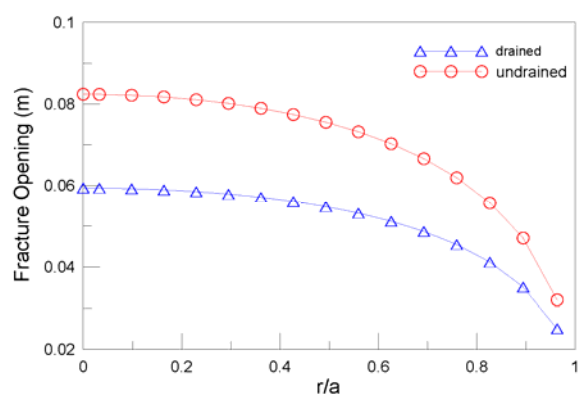

Figure 6: Long term and short term fracture opening profiles in response to combined mode 1 and 2 loading; "r" is distance to the point and "a" is the radius of the fracture.

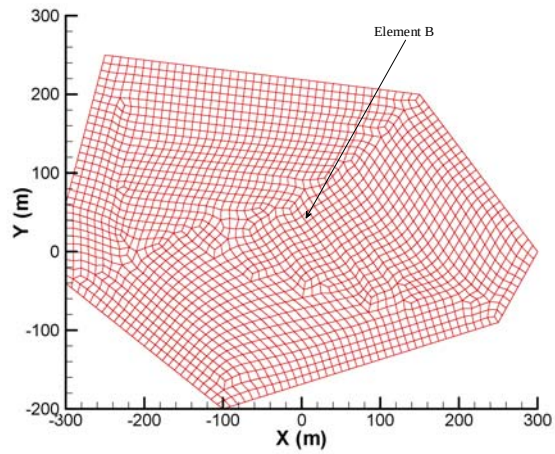

Figure 7: Discretization of irregular fracture using four-noded quadrilateral elements.

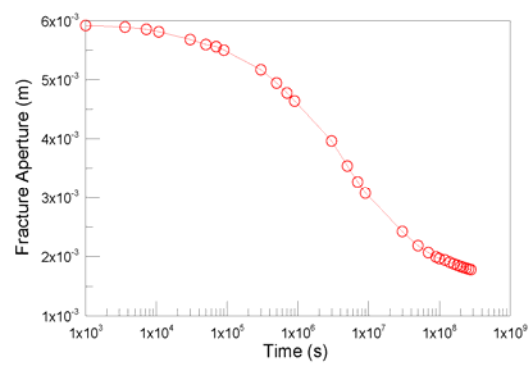

Figure 8: Variation of fracture aperture on element B with time.

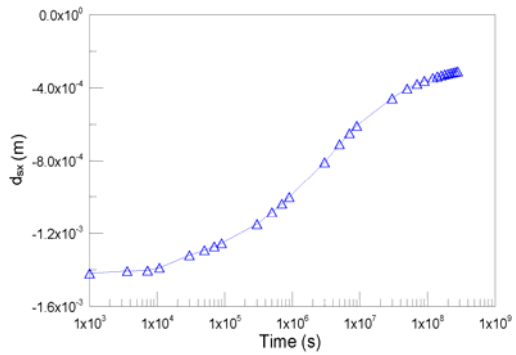

Figure 9: Variation of slip in x-direction for element B with time.

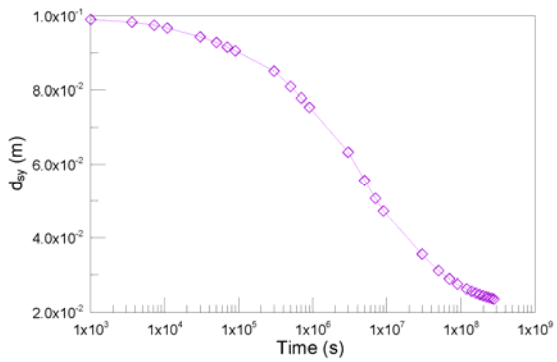

Figure 10: Variation of slip in y-direction for element B with time.

CONCLUSIONS

A three-dimensional displacement discontinuity method has been developed to analyze the behavior of the fracture opening and slip in response to the application of fluid pressure in the fracture. The field quantities such as solid displacement, fluid flux, stress and pore pressure, are evaluated by using the integral equation method in terms of the densities of the discontinuous solid displacement and fluid flux across the fracture. Using these boundary integral equations, we only need to discretize the fracture surface instead of the whole domain. The natural fracture deformation was assumed to be linear elastic and considered dilation related to the fracture slip which was modeled using Mohr-Coulomb criterion.

The three-dimensional model was applied to study the poroelastic response of the fracture opening and slip. It was found that the application of the normal stress loading causes the increase of the fracture opening with the time because of the dissipation of the pore pressures in the rock; while the pore pressure

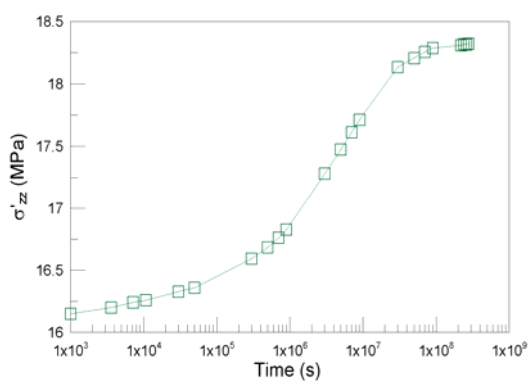

Figure 11: Variation of normal effective stress for element B with time.

loading causes the increase of the fracture closure due to fluid leak-off from the fracture into the rock. This is consistent with previous studies (Ghassemi and Roegiers, 1996; Detournay and Cheng, 1993).

Often, field applications involve injection pressures that are insufficient to jack the fracture open. Simulation of this scenario shows that application of the fluid pressure in a fracture under critical shear stresses causes the fracture to slip and dilate. Thereafter, the fracture slip decrease as the matrix dilation caused by pore pressure diffusion increases the normal stress on the fracture surface, and reduces the dilation induced crack opening. Such a transient slip can be manifested in injection pressure variations as well in induced reservoir seismicity observed in enhanced or engineered geothermal systems.

ACKNOWLEDGEMENTS

This project was supported by the U.S. Department of Energy Office of Energy Efficiency and Renewable Energy under Cooperative Agreement DE-FG36-06GO95002. This support does not constitute an endorsement by the U.S. Department of Energy of the views expressed in this publication.

REFERENCES

Biot, M.A. (1941). General Theory of Three-Dimensional Consolidation. *Journal of Applied Physics*. Vol. 12, pp. 155-169.

Carter, J.P. and Booker, J.R. (1982). Elastic consolidation around a deep circular tunnel. *Int. J. Solids Structures*. Vol. 18(12), pp. 1059-1074

Carvalho J. and Curran J.H. (1998). Three-dimensional displacement discontinuity solutions for

fluid-saturated porous media. *Int. J. Solids Structures*. Vol. 35, pp. 4887-4893.

Cheng, A.H.-D. and Detournay, E. (1998). On singular integral equations and fundamental solutions of poroelasticity. *Int. J. Solids Structures*. Vol. 35, pp. 4521–4555.

Crouch, S.L. and Starfield, A.M. (1983). Boundary element methods in solid mechanics, Allen Unwin, NY.

Detournay, E. and Cheng, A. H.-D. (1993). Fundamentals of poroelasticity. In: Comprehensive rock engineering: principles, practice and projects, analysis and design method. Vol 2. Editor: C. Fairhurst. Pergamon Press, Oxford. 113-171.

Ghassemi, A. and Roegiers, J.-C. (1996). "A three-dimensional poroelastic hydraulic fracture simulator using the displacement discontinuity method," Proc. 2nd North American Rock Mech. Symposium, Montreal, Ca, **1**, 982-987.

Ghassemi, A., Tarasovs, S. and Cheng, A. H.-D. (2007). "A Three-Dimensional Study of the Effects of thermo-mechanical loads on fracture slip in enhanced geothermal reservoir," *Int. J. Rock Mechanics & Min Sci*., Vol. 44 , pp. 1132–1148.

Gordeyev, Y. (1993). Growth of a crack produced by hydraulic fracture in a poroelastic medium, *International Journal of Rock Mechanics and Mining Sciences & Geomechanics Abstracts*, Vol. 30 (3), pp. 233-238.

Rice, J.R. and Cleary, M.P. (1976). Some basic stress diffusion solutions for fluid-saturated elastic porous media with compressible constituents. *Reviews of Geophysics and Space Physics*. Vol. 14, pp. 227-241.

Vandamme, L., and Curran, J.H. (1989). A three-dimensional hydraulic fracturing simulator. *Int. J. Numer. Methods Eng*. Vol. 28, pp. 909-27.